ELSEVIER

Journal of Biomechanics 37 (2004) 613–621

JOURNAL OF BIOMECHANICS

www.elsevier.com/locate/jbiomech
www.JBiomech.com

Finite element models predict cancellous apparent modulus when tissue modulus is scaled from specimen CT-attenuation

Benjamin C. Bourne[a], Marjolein C.H. van der Meulen[a,b,*]

[a] *Sibley School of Mechanical and Aerospace Engineering, Aerospace Engineering, Cornell University, 219 Upson Hall, Ithaca, NY 14853-7501, USA*
[b] *Laboratory for Biomedical Mechanics and Materials, Hospital for Special Surgery, New York, NY 10021, USA*

Accepted 8 October 2003

Abstract

High-resolution architecture-based finite element models are commonly used for characterizing the mechanical behavior of cancellous bone. The vast majority of studies use homogeneous material properties to model trabecular tissue. The objectives of this study were to demonstrate that inhomogeneous finite element models that account for microcomputed tomography-measured tissue modulus variability more accurately predict the apparent stiffness of cancellous bone than homogeneous models, and to examine the sensitivity of an inhomogeneous model to the degree of tissue property variability. We tested five different material cases in finite element models of ten cancellous cubes in simulated uniaxial compression. Three of these cases were inhomogeneous and two were homogeneous. Four of these cases were unique to each specimen, and the remaining case had the same tissue modulus for all specimens. Results from all simulations were compared with measured elastic moduli from previous experiments. Tissue modulus variability for the most accurate of the three inhomogeneous models was then artificially increased to simulate the effects of non-linear CT-attenuation-modulus relationships. Uniqueness of individual models was more critical for model accuracy than level of inhomogeneity. Both homogeneous and inhomogeneous models that were unique to each specimen had at least 8% greater explanatory power for apparent modulus than models that applied the same material properties to all specimens. The explanatory power for apparent modulus of models with a tissue modulus coefficient of variation (COV) range of 21–31% was 13% greater than homogeneous models (COV = 0). The results of this study indicate that inhomogenous finite element models that have tissue moduli unique to each specimen more accurately predict the elastic behavior of cancellous cubic specimens than models that have common tissue moduli between all specimens.

Keywords: Cancellous bone; Finite element; Modulus; Microcomputed tomography; Tissue properties

1. Introduction

Cancellous bone plays an important role in the load-bearing function of the skeleton, and is significantly impacted when diseased. Several studies have used architecture-based models to predict the mechanical behavior of cancellous bone in uniaxial compression (van Rietbergen et al., 1995; Ulrich et al., 1997; Ladd et al., 1998; Kabel et al., 1999). While these models provide an accurate structural representation of the architecture, they assume isotropic, homogeneous, and linear elastic trabecular tissue properties and do not account for quantitative and spatial property variability. However, the elastic behavior of cancellous bone is likely a function of not only quantity and architecture, but also of tissue material properties.

Characterizing the contributors to elastic behavior is difficult, as researchers have shown that cancellous bone is not only architecturally anisotropic, but is also a complex composite at the microstructural and ultra-structural levels. While evidence of structural and tissue property differences exists in cortical bone across animal species (Currey, 1988) and across anatomic location (Hobatho et al., 1997; Hoffler et al., 2000), the nature of these variations within a single cancellous specimen is poorly understood. Several recent studies show that

*Corresponding author. Sibley School of Mechanical and Aerospace Engineering, Aerospace Engineering, Cornell University, 219 Upson Hall, Ithaca, NY 14853-7501, USA. Tel.: +1-607-255-1445; fax: +1-607-255-1222.
E-mail address: mcv3@cornell.edu (M.C.H. van der Meulen).

0021-9290/$ - see front matter © 2003 Elsevier Ltd. All rights reserved.
doi:10.1016/j.jbiomech.2003.10.002

these properties vary locally throughout lamellar trabecular bone: Paschalis et al. (1997) have shown that tissue mineralization varies spatially within trabecular bone, decreasing near trabecular surfaces; collagen fiber orientation has been shown to be primarily longitudinal in lamellar bone, but varies within lamellar interface regions (Weiner et al., 1997; Ziv et al., 1996); and hydroxyapatite crystals, of which the elastic properties depend on crystal orientation, are predominantly aligned with collagen fibers (Ziv et al., 1996). Furthermore, these variations appear to be consistent with the two principles that formation of cancellous bone takes place on trabecular surfaces, and that newly produced collagenous tissue becomes more mineralized and rigid with age. The result is an inhomogeneous mineral distribution that should cause tissue density, and thus tissue modulus, to increase from trabecular surface to core.

Two recent studies have applied arbitrarily determined tissue-property inhomogeneity to high-resolution image-based architectural finite element models (van der Linden et al., 2001; Jaasma et al., 2002). These studies demonstrated that an architectural model that accounts for tissue inhomogeneities predicts a lower apparent modulus than is predicted by homogeneous models. However, these finite element models implemented arbitrary choice of reference tissue modulus and spatial property distributions. With microCT, we recently observed variable tissue attenuation within cancellous bone that is consistent with surface tissue formation (Bourne et al., 2002; Morgan et al., 2002). Although the mean tissue X-ray attenuation was approximately 20% lower than the level in cortical bone (Fig. 1), attenuation was 17% lower at the trabecular core and, more importantly, dropped to 68% of interstitial cortical tissue attenuation at the trabecular surface (Fig. 2, Morgan et al., 2002).

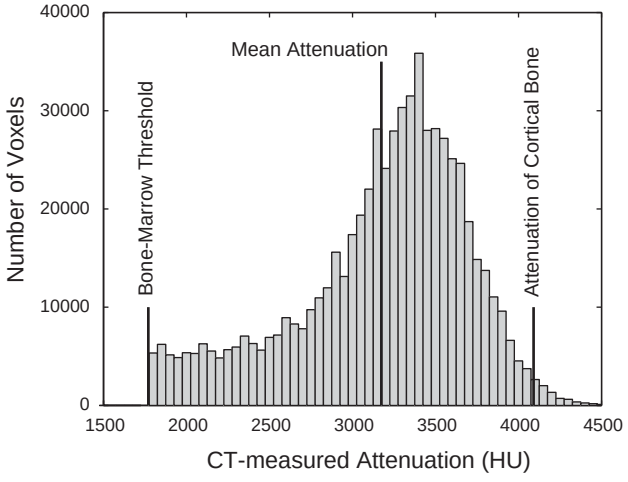

Fig. 1. Quantitative distribution of thresholded CT attenuation values for a single cancellous specimen scanned by microCT (33 μm cubic voxels, $CT_{threshold} = 1770$ HU, $CT_{mean} = 3174$ HU, $CT_{cortical} = 4091$ HU).

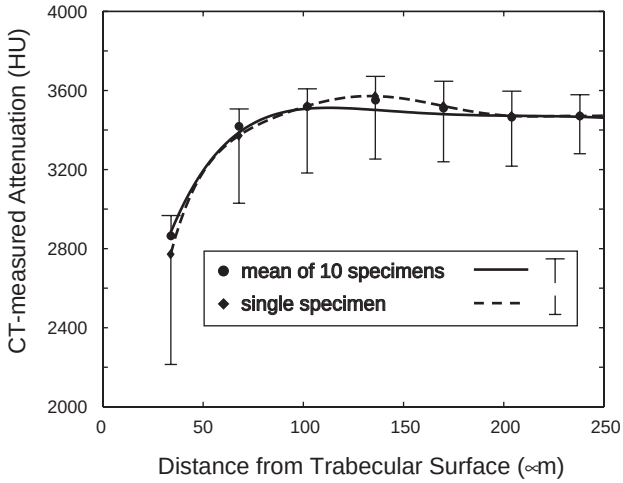

Fig. 2. Spatial distribution of thresholded CT attenuation (33 μm cubic voxels) as a function of distance from trabecular surface for a single specimen (dashed) and 10 specimens (solid). Data are shown with standard deviations, and fit with sixth-order polynomials.

These material mineralization measures demonstrate that trabecular tissue properties vary both quantitatively and spatially within a single specimen. However, the magnitude of the elastic trabecular tissue modulus historically has been approximated using the modulus of interstitial cortical bone. Several studies have quantified the properties of trabecular and cortical tissue. While some early micro-bending and tensile estimates of elastic modulus in lamellar bone were in the range of 3–5 GPa (Choi et al., 1990; Kuhn et al., 1989), Burstein et al. (1975) reported values as high as 20–28 GPa for partially to fully calcified cortical bovine specimens loaded in uniaxial tension. Recent studies using nanoindentation reported measurements that agree more closely with Burstein's results, with tissue indentation modulus values between 8.0 and 31.6 GPa for cancellous bone (Rho et al., 1997, 1999; Turner et al., 1999; Zysset et al., 1999; Hoffler et al., 2000; Hengsberger et al., 2002). This wide range of reported values likely demonstrates the presence of spatial variability in tissue modulus. Most data, besides Hoffler et al. (2000), indicate that trabecular tissue properties are similar to those of cortical bone.

In this study, we hypothesized that the cancellous architecture alone would be insufficient to fully capture the experimental elastic behavior in finite element simulations. In particular, we hypothesized that inhomogeneous finite element models that account for spatial elastic property variations would more accurately simulate experimental compression tests than models that assumed homogeneous, isotropic tissue properties. We used the local spatially varying X-ray attenuation measured by microCT scans to examine the

relative ability of homogeneous and inhomogeneous tissue material property distributions to accurately capture the elastic behavior of cancellous cubes as measured from experimental tests.

2. Materials and methods

Three-dimensional microCT images from five pairs of previously tested then scanned cancellous specimens (Bourne et al., 2002) were used to construct trabecular architecture-based finite element models for simulated mechanical testing. Ten paired 4-mm cubes were excised from the medial ($n = 5$) and lateral ($n = 5$) femoral condyles of skeletally mature New Zealand White rabbits. Experimental specimens were loaded in uniaxial compression to approximately 0.65% strain along the inferior–superior axis, and apparent elastic modulus was measured for each cube. Micro-computed tomography scans of each specimen (MS-8 Small Specimen Scanner, Enhanced Vision Systems, London, Ontario) were reconstructed at 16.3-μm isotropic resolution and globally thresholded to distinguish bone from marrow voxels.

Finite element models were constructed directly from the microCT data. Each scan was coarsened by combining eight adjacent voxels into a single 33-μm voxel and averaging the eight CT-attenuation values. The voxel size and cube dimensions of our models satisfied the continuum assumption for a porous material (Homminga et al., 2001). To ensure that the outer surfaces of each finite element model corresponded to voxel surfaces, a 3.8-mm sub-region of each image was trimmed from the original 4-mm cubic image. Image voxels were then converted to isotropic, 8-noded cubic brick elements with unique X-ray attenuation values. Following removal of disconnected elements, cubic models contained between 5.7×10^5 and 8.1×10^5 brick elements.

An element-by-element finite element solver was used to perform uniaxial compression simulations (van Rietbergen et al., 1995, 1996). The prescribed displacement matched the experimental displacement for each respective specimen, and was equivalent to 0.58–0.68% strain. Boundary constraints simulated a frictionless interface between the specimen and loading platens. Poisson's ratio was assumed to be 0.3 for all elements. Each simulation required approximately 2500 iterations and two hours of computation time (Compaq XP1000, 667 MHz, 1GB RAM, Houston, TX).

2.1. Variable tissue modulus

To test our hypothesis that inhomogeneous models more accurately predict experimental behavior than homogeneous models, simulations were performed using five tissue modulus relationships (Table 1). Each case was classified as either specimen-specific (unique architecture and tissue modulus distribution for each specimen) or non-specimen-specific (unique architecture, but common tissue property distribution between specimens), and cases ranged from homogeneous non-specimen-specific to inhomogeneous specimen-specific. Apparent moduli from these five tissue modulus cases were compared with the previously measured experimental values for the ten specimens.

Table 1
Five tissue modulus cases implemented in architecture-based finite element models. Each case is specified with either a homogeneous or inhomogeneous tissue modulus distribution, and as either specimen-specific or common across all specimens

Tissue modulus case	Tissue modulus distribution	Specimen specificity?
Modulus as a function of measured tissue attenuation (E_{CT2E})	Inhomogeneous	Yes
Modulus as a function of distance from nearest surface (E_{Dist})	Inhomogeneous	Yes
Modulus as a function of mean attenuation (E_{aveCT})	Homogeneous	Yes
Modulus as a function of averaged distance from nearest surface ($E_{aveDist}$)	Inhomogeneous	No
Reference modulus ($E_{20\,GPa}$)	Homogeneous	No

In addition to architectural information, a microCT scan provides a unique X-ray attenuation value for each voxel in the three-dimensional structural model. This attenuation may be converted into local tissue density at each voxel, and then into a corresponding local tissue modulus as input for the finite element model. We thus had measured density from microCT scans of our experimentally tested cubic specimens, and used these density values to develop the different tissue property cases for comparison with measured experimental results.

The inhomogeneous tissue density case (E_{CT2E}) used a linear attenuation-to-tissue modulus relationship to assign a unique microCT-based tissue modulus to each bone voxel in the specimen. This linear distribution was scaled about a 20 GPa reference tissue modulus chosen as the representative stiffness of interstitial lamellar bone, with a tissue density of 1.1 g/cc. This tissue density corresponded to an X-ray attenuation of 4091 Hounsfield Units (HU). When applied to the attenuation data for our cubic specimens, this linear scaling resulted in a tissue modulus range of 8.1–24.3 GPa, with a coefficient of variation (COV = standard deviation/mean) of 13.9–18.7%. The skewed distribution of attenuation values below the 4091 HU reference attenuation caused the mean tissue modulus for all inhomogeneous cases to be lower than the 20 GPa reference value for all cubes (14.6–16.3 GPa, Fig. 1).

Due to the similarity in spatial attenuation distribution between cubes (Fig. 2), we tested a second inhomogeneous tissue density case (E_{Dist}) using a specimen-specific attenuation. This distribution case, based on a distance transformation (Jain, 1989), assigned to each voxel in the model an integer value representing its distance from the nearest trabecular surface. For each specimen, a sixth-order polynomial function was fit to the data for mean CT-attenuation (Fig. 2). Based on this closed-formed relationship, a non-integer attenuation value was then assigned to each node in the model according to this mean CT-distance relationship. A tissue modulus at each node was calculated using the same linear relationship as the microCT-to-tissue modulus case (E_{CT2E}). The mean specimen-specific tissue modulus and COV ranges for these models were 13.3–18.4 GPa and 7.3–10.5%, respectively. A third inhomogeneous case ($E_{aveDist}$) was developed to apply a common attenuation distribution to all cubes in the group. This was done by averaging the specimen-specific mean attenuation values from the E_{Dist} case for all cubes at each depth from surface, and again fitting a sixth-order polynomial to these mean values (Fig. 2). The tissue modulus and COV ranges for this distribution across all cubes were 14.2–18.3 GPa and 7.0–7.6%, respectively.

We then investigated the accuracy of two homogeneous modulus cases. The first (E_{aveCT}) was a specimen-specific model that assigned the mean tissue modulus from inhomogeneous case E_{CT2E} to each element (14.6–16.3 GPa). The second homogeneous case ($E_{20\,GPa}$) assumed that all lamellar trabecular bone had elastic properties identical to interstitial cortical bone, and therefore applied a single tissue modulus of 20 GPa to all bone elements in the 10 specimen models. These two homogeneous cases resulted in purely architectural simulations for which the resultant apparent modulus for each specimen was a scalar multiple of both prescribed displacement and assigned tissue modulus.

2.2. Variability in tissue modulus

If a significant number of trabeculae in a single specimen are subjected to bending loads, then the distribution of tissue moduli from core to trabecular surface would have a significant effect on specimen stiffness. This bending becomes more pronounced as the difference between modulus at the trabecular surface and at the trabecular core increases. Several studies have shown that the apparent modulus of cancellous bone may be related to mineral content and to apparent density of a tested volume of bone through approximately linear, quadratic and cubic relationships (Carter and Hayes, 1977; Keaveny et al., 1994; Hobatho et al., 1997). Rho et al. (1993) reported that such a power relationship may be extrapolated to calculate tissue modulus from tissue density. Clearly, the nature of this mineral–modulus relationship dictates the amount of variability in tissue modulus distribution. We investigated the sensitivity of model results to the degree of tissue modulus variability about the reference tissue modulus (20 GPa). By increasing the slope of our previous linear relationship between CT number and tissue modulus about the known density and modulus of interstitial lamellar bone (4091 HU and 20 GPa), we effectively captured the near-linear distribution of moduli about the reference tissue modulus for exponents greater than unity (Fig. 3). Three distinct tissue modulus and coefficient of variation ranges were examined by increasing the slope for each variable tissue modulus case:

for $s = 1.0$, $E_{tissue} = 8.1-24$ GPa (COV = 13−18%) and $E_{mean} = 14-16$ GPa,

for $s = 1.4$, $E_{tissue} = 3.1-26$ GPa (COV = 21−30%) and $E_{mean} = 13-15$ GPa,

for $s = 1.7$, $E_{tissue} = 0.3-27$ GPa (COV = 28−40%) and $E_{mean} = 11-14$ GPa,

where s is the slope multiplier, E_{tissue} and COV are the resulting ranges of tissue modulus and corresponding variability, and E_{mean} is the average tissue modulus range across the 10 distinct finite element models. Consistently, minimum and mean tissue modulus decreased, and maximum tissue modulus increased with increasing tissue modulus distribution range (Fig. 4). To determine the most effective distribution for predicting

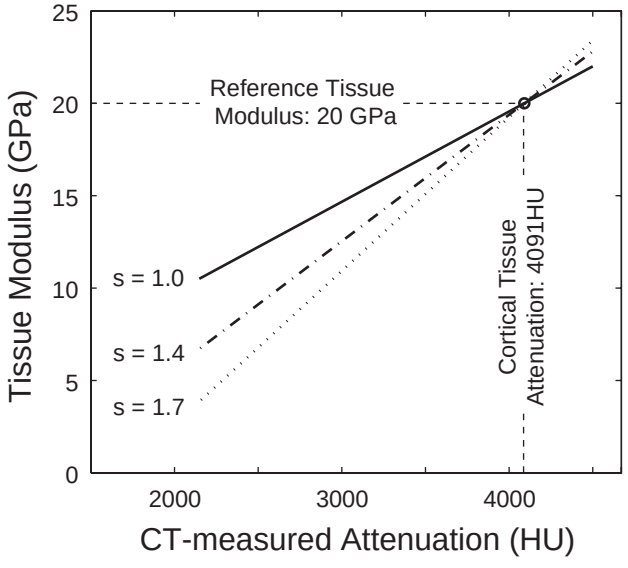

Fig. 3. Three ranges of linear tissue modulus distribution about a 20 GPa reference modulus and a reference cortical tissue attenuation of 4091 HU for different slope multipliers, s: $s = 0$ (COV = 0), $s = 1$ (COV = 14−19%), $s = 1.4$ (COV = 21−30%), and $s = 1.7$ (COV = 28−40%). Linear distribution $s = 1.0$ passes through the origin, while $s = 1.4$ and 1.7 represent the near-linear segments of higher-order attenuation-to-tissue modulus relationships.

experimental behavior, the predicted apparent moduli of these three ranges were compared with experimental moduli.

2.3. Statistical analysis

Following all simulations, a repeated measures ANOVA was performed to: (1) identify significant differences in apparent modulus between modulus cases, between medial and lateral specimens (as was found in experimental results), and between simulation and experimental results, and (2) determine the sensitivity of apparent modulus results for the attenuation-to-tissue modulus case to increasing tissue modulus variability. All averaged results are reported with standard deviations, and statistical significance was defined as $p<0.05$.

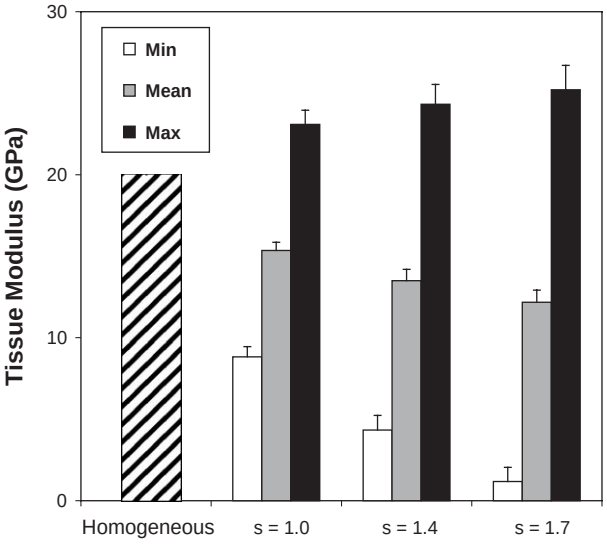

Fig. 4. Three ranges of linear tissue modulus distribution about a 20 GPa reference modulus and a reference cortical tissue attenuation of 4091 HU for different slope multipliers, s: $s=1.0$ (COV = 13.9−18.7%), $s=1.4$ (COV = 21.4−30.5%), and $s=1.7$ (COV = 28.1−40.1%). Mean values shown with standard deviation ($n=10$).

3. Results and analysis

3.1. Variable tissue modulus

The apparent modulus predicted by the 20 GPa model was significantly greater than the modulus for the other four cases ($p<0.001$), and overpredicted experimental modulus in every specimen (Fig. 5). The means results for the four other cases were not significantly different from the experimental apparent modulus, but the individual results for each case demonstrated substantial variability between specimens ($p<0.001$). All models successfully captured the significant stiffness differences between lateral and medial specimens found in earlier experiments (Fig. 5; $E_{\text{lateral}}<E_{\text{medial}}$, $p<0.001$). Linear regressions showed that the three specimen-specific models (E_{CT2E}, E_{Dist}, E_{aveDist}) explained up to 9% more of the experimental apparent modulus than either non-specimen-specific model (E_{aveCT}, $E_{20\,\text{GPa}}$; Fig. 6a).

3.2. Variability in tissue modulus

A greater distribution of tissue modulus values about the 20 GPa reference modulus caused a non-linear

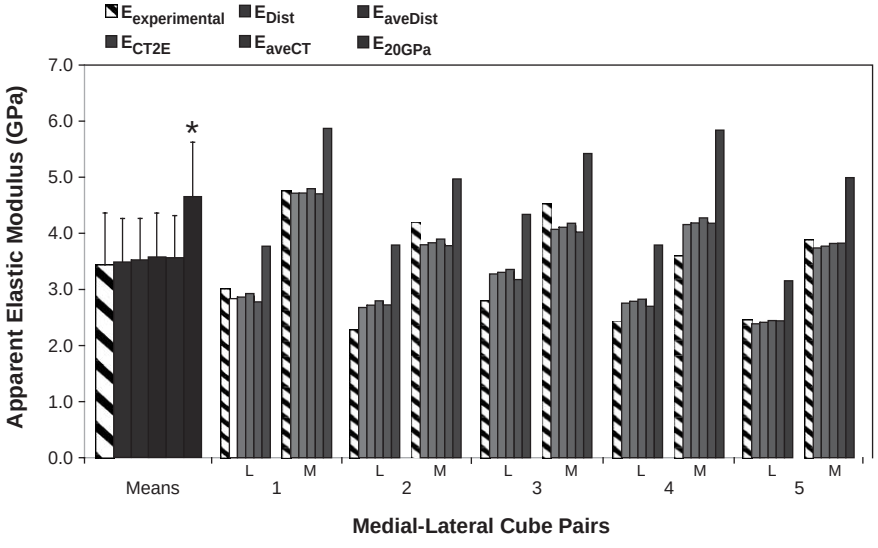

Fig. 5. Apparent modulus results for experimental uniaxial compression tests of cancellous cubes ($n=10$, 5 Medial, 5 Lateral) and five different finite element models for the same 10 specimens. Mean values shown with standard deviations. *Apparent modulus for the 20 GPa homogeneous model was significantly greater than all other model results ($p<0.001$).

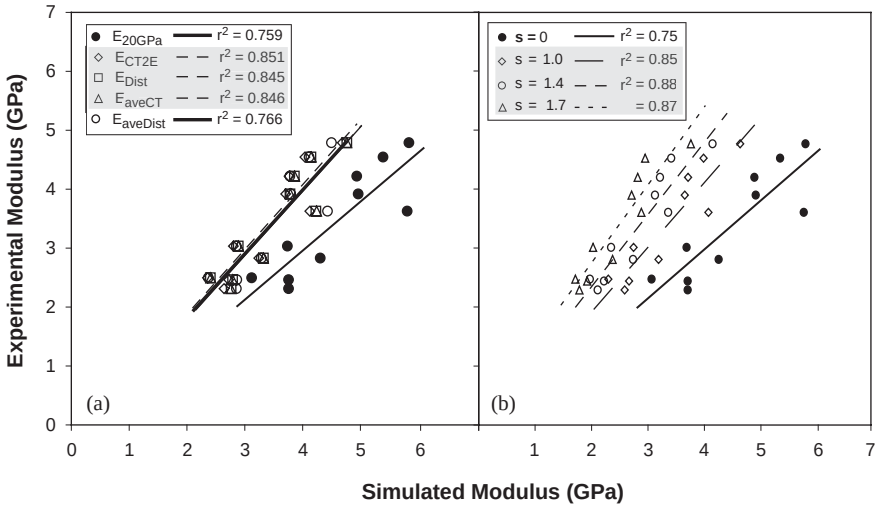

Fig. 6. (a) Relative effectiveness of five finite element models in predicting the elastic behavior of cancellous cubes. Specimen-specific models (E_{CT2E}, E_{Dist}, E_{aveCT}) was at least 8% more effective for predicting apparent modulus than specimen-common models ($E_{20\,GPa}$, $E_{aveDist}$). (b) Effect of increasing tissue modulus variability on the predictive power of an inhomogeneous tissue modulus model for apparent modulus in cancellous specimens. Results are shown for four different linear slope multipliers, s: $s = 1.0$ (COV = 13.9−18.7%), $s = 1.4$ (COV = 21.4−30.5%), and $s = 1.7$ (COV = 28.1−40.1%), and indicate that a linear X-ray-attenuation-to-tissue modulus relationship ($s = 1$, $r^2 = 0.85$) less precisely predicts experimental modulus than a higher-order relationship ($s = 1.4$, $r^2 = 0.88$). Simple linear regression are shown for simulations performed on 10 specimens. Shaded values represent $r^2 > 0.80$.

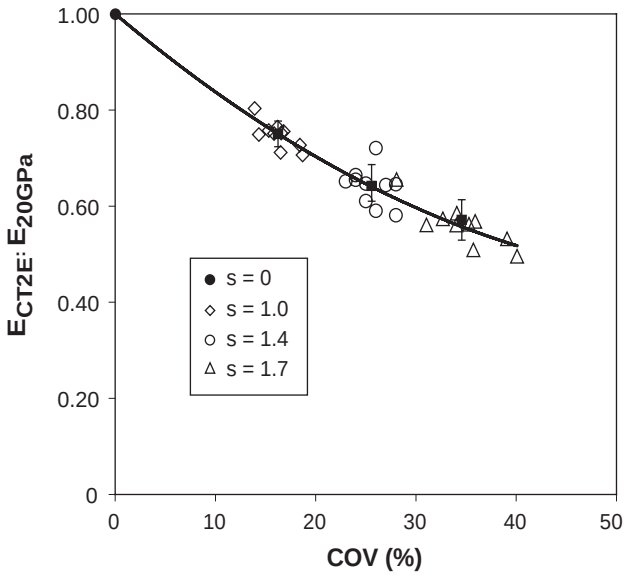

Fig. 7. Effect of increasing tissue modulus variability on simulated apparent modulus. Apparent moduli for inhomogeneous tissue modulus case normalized by 20 GPa homogeneous tissue modulus shown for four linear scales: $s = 0$ (COV = 0), $s = 1.0$ (COV = 13.9−18.7%), $s = 1.4$ (COV = 21.4−30.5%), and $s = 1.7$ (COV = 28.1−40.1%), where s is the slope multiplier. Increases in COV of 16%, 26%, and 34% resulted in 24%, 35%, and 43% reductions in predicted apparent modulus, respectively. Modulus means are shown as solid squares with standard deviations, and are significantly different between each distribution range (0, 1.0, 1.4 and 1.7; $p < 0.001$).

decrease in simulated apparent modulus with respect to that of the homogeneous 20 GPa model. On average, 16%, 26%, and 34% increases in COV resulted in approximately 26%, 35%, and 43% reductions in predicted apparent modulus for the inhomogeneous attenuation-to-tissue modulus case (Fig. 7). This trend was best fit with a second-order polynomial for the mean modulus ($r^2 = 0.93$). When analyzed separately by location (medial, lateral), a second-order curvefit allowed apparent modulus of specimens from the medial condyle to be predicted with greater accuracy ($r^2 = 0.96$) than that of lateral specimens ($r^2 = 0.93$). Inhomogeneous model results (slope multiplier = 1.0, 1.4 and 1.7) all had high explanatory power for experimental elastic modulus ($r^2 > 0.85$). The intermediate range ($s = 1.4$, COV = 21−30%) most precisely predicted experimental modulus among the three ranges examined (Fig. 6b).

Finally, the role of an inhomogeneous tissue modulus distribution in predicting elastic behavior in a cancellous cube was more significant with increasing tissue modulus variability. Much of this effect was due simply to the lower mean modulus in the simulations with increased variability. The contribution of increasing tissue variability was examined by normalizing each tissue modulus distribution result by its mean modulus (Fig. 8). As the variability increased, the contribution of the tissue inhomogeneity increased. For the maximum variability range ($s = 1.7$), 12% of the total 45% apparent modulus reduction was due to this variability (Figs. 7 and 8).

4. Discussion

Characterizing the mechanical properties and structural behavior of normal cancellous bone is essential for

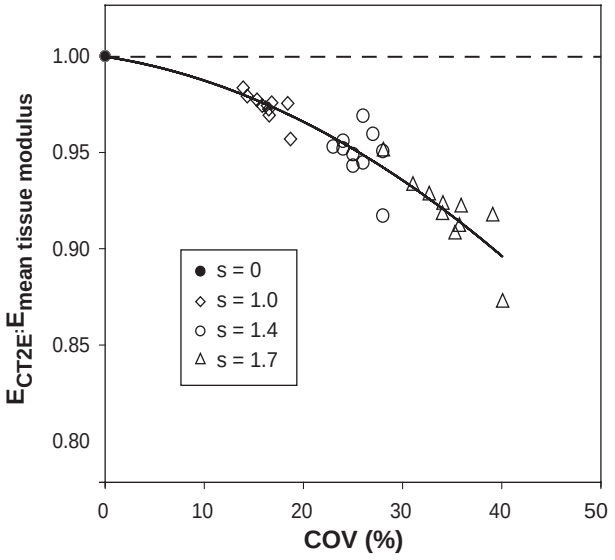

Fig. 8. Role of a homogeneous mean tissue modulus model with respect to an inhomogeneous variable tissue modulus model in predicting apparent modulus in cancellous cubes. Ratio of apparent moduli for inhomogeneous tissue modulus case normalized by 20 GPa homogeneous tissue modulus is shown for four linear scales: $s = 0$ (COV = 0), $s = 1.0$ (COV = 13.9−18.7%), $s = 1.4$ (COV = 21.4−30.5%), and $s = 1.7$ (COV = 28.1−40.1%), where s is the slope multiplier. A model dependent only on mean tissue modulus would have a value of 1 (dashed line). The role of an inhomogeneous tissue modulus distribution became more important with increasing variability.

assessing potentially diseased cancellous bone using a non-invasive clinical technique. The objective of this study was to demonstrate that finite element models with inhomogeneous tissue properties derived from experimental measurements are better predictors of apparent modulus in cancellous bone than models that do not account for local tissue modulus variability. This objective was addressed by (1) comparing the ability of various finite element models that incorporate variable tissue properties to predict cancellous bone mechanical behavior in uniaxial compression, and (2) isolating the significance of increasing tissue modulus variability on the prediction of this behavior. Our results demonstrate that a specimen-specific model is a better predictor of experimental apparent modulus than a single model applied to all specimens. We have also shown through the variability study that, while the predicted apparent modulus is heavily influenced by the mean tissue attenuation of the individual specimen, this predicted modulus is also dependent on the amount of tissue modulus variability about the mean value.

This is the first study to use measured inhomogeneities from CT-attenuation to compare the performance of inhomogeneous and homogeneous computational models for predicting the structural behavior of cancellous bone specimens. Our results indicate that uniqueness of tissue properties between specimens is more important than cube inhomogeneity for predicting elastic response to uniaxial loading at low tissue modulus variability. We also found that at higher levels of variability, an inhomogeneous specimen-specific model predicted a lower apparent modulus than a homogeneous model with the same mean tissue modulus. This result is similar to that of a recent study by Jaasma et al. (2002), in which a linear surface-formation based mineral distribution was applied to an architectural finite element model. However, the percent reduction in apparent modulus predicted by the inhomogeneous model in this study was approximately 50% less than that predicted by Jaasma et al. This difference is likely attributed to the skewed distribution of tissue attenuation values measured in our specimens (Fig. 1), while Jaasma et al. used a hypothetical normal distribution about a mean tissue modulus. These results confirm that apparent modulus predicted by the tissue attenuation-to-modulus model (E_{CT2E}) is not dependent only on the mean tissue modulus.

Using a function to map attenuation to tissue modulus did not justify the additional computational effort required to implement these simulations. The E_{Dist} case was the least effective of the specimen-specific models, and the averaged case ($E_{aveDist}$) was 8% less effective at predicting experimental modulus than the former. Therefore, assigning CT-attenuation values to model elements based on a common distance-to-surface function was less effective than using either an inhomogeneous or homogeneous mean tissue modulus, specimen-specific model.

A number of earlier studies have been conducted in which results of finite element simulations were compared to experimental tests of architecturally and compositionally identical specimens taken from human vertebrae, human femora, bovine femora, and whale vertebrae (Ulrich et al., 1997; Kabel et al., 1999; Ladd et al., 1998). Each of these comparative studies, however, assumed homogeneous, isotropic tissue properties, and calculated an effective isotropic tissue modulus based on apparent modulus simulation results in three orthogonal directions (Ulrich et al., 1997). These calculated tissue moduli ranged from 3.5–8.6 GPa, and experimental measurements from additional studies resulted in apparent moduli of approximately 4.5 GPa (Choi et al., 1990; van Lenthe et al., 2001). While our choice of a 20 GPa reference tissue modulus is 2.3–5.7 times greater than that found in previous studies, our experimental apparent moduli ranged from 2.3 to 4.8 GPa, compared with previously reported 0.1–0.7 GPa. Finally, van der Linden et al. (2001) hypothesized that variability in previous nanonindentation results could result from the formation-based distribution of tissue properties. These and other studies demonstrate the strong dependence of cancellous

mechanical performance on animal species (Currey, 1984), anatomic location (Hobatho et al., 1997), and age (Ladd et al., 1998), among many other potential factors. Thus, comparison with the results of other studies must be limited to the effectiveness of a model to predict behavior within the group of the respective study.

The primary strengths of this study were the use of measured attenuation to determine tissue properties for model input, and the comparison of simulation results with those of previously conducted experiments on the same cubic specimens. Other studies have relied on estimates of tissue modulus based on orthogonal compressive moduli (van Rietbergen et al., 1996; Ulrich et al., 1997; Kabel et al., 1999) and hypothetical property distributions (van der Linden et al., 2001; Jaasma et al., 2002). The microCT scans in our study provided true and unique CT-attenuation distributions for each cube modeled. Furthermore, our use of a constant reference tissue modulus corresponding to the CT-attenuation of interstitial cortical bone allowed us to maintain the true distribution of tissue attenuation within and between specimens. We were then able to compare the results of our finite element simulations with those of the same previously tested cubes, which showed variability in several parameters: architecture, location (medial–lateral), tissue property distribution, and apparent elastic modulus. Our models successfully captured this variability across the group of tested specimens.

This study provides insight to the results of several earlier studies, but is not without limitations. We chose 20 GPa as a representative tissue modulus for interstitial lamellar bone to correspond to a mineral density of 1.1 g/cc (X-ray attenuation of 4091 HU). While this value remained constant for all cubes and models, a higher-exponent power law (greater than unity) used to calculate tissue modulus from tissue attenuation values would require a lower reference tissue modulus to match our simulation results with experimentally measured apparent modulus. Thus, the results of our variability study are only valid for this reference tissue modulus of 20 GPa, and for a narrow range of experimental modulus results (2.3–4.8 GPa).

Our models more accurately represented the mineralization variability within trabecular tissue than was represented in previous studies, but did not fully capture the structural behavior of cubic specimens. Simulation results for several specimens had low variability for the attenuation-based model. However, the predicted apparent modulus for other specimens had greater variability with respect to experimentally measured apparent modulus (Fig. 5), similar to the results of an earlier study by Ulrich et al. (1997). This implies that additional differences exist between intra-specimen factors that were not considered in our models. First, grouping adjacent voxel tissue properties for reducing computation time may compromise the accuracy of the models, particularly in regions of lower attenuation close to trabecular boundaries. Our technique of applying measured attenuation values to finite element models of cancellous bone will likely improve as the limits of computational capabilities expand to accept larger number of mesh elements, and as the trabecular attenuation-to-modulus relationship becomes more accurate. Second, microCT measures a homogeneous, isotropic attenuation value for each voxel in the scan volume, and cannot detect variations in the ultrastructure of trabecular tissue (e.g. mineral crystal and collagen orientation). This ultrastructural simplification will become significant with increases in scanning resolution of microCT and other imaging techniques (van Rietbergen et al., 2002).

We have shown in this study that (1) specimen-specific finite element models that scale cancellous tissue modulus with microCT attenuation are more effective predictors of cancellous mechanical behavior than general models that apply identical tissue properties to all specimens in the group, and that (2) homogeneous, specimen-specific models predict increasingly greater apparent moduli than inhomogeneous models for increasing coefficient of variation in tissue modulus. Thus, incorporating variability in tissue properties into predictive models of cancellous bone is important for achieving accurate apparent-level results. Because we are now able to apply a measured tissue attenuation value to each voxel in the finite element model, the accuracy of the specimen-specific model is now limited by the conversion relationships between CT-measured attenuation, tissue mineralization, and elastic modulus. Given an accurate and proven measure for reference tissue modulus of interstitial lamellar bone, the results of our variability study may provide an effective method for future derivation of an accurate attenuation-to-modulus relationship through the correlation of experimental and computational results.

Acknowledgements

The authors thank Timothy Morgan for scanning the specimens and for his technical assistance, and Dr. Harrie Weinans of Erasmus Universiteit Rotterdam for the element-by-element finite element solver code. This study was supported by a grant from The Whitaker Foundation (RG-99-0053).

References

Bourne, B.C., Morgan, T.G., Paschalis, E., van der Meulen, M.C., 2002. Cancellous bone anisotropy arises from both architecture

and material properties. Transactions of the Orthopaedic Research Society 27, 558.

Burstein, A.H., Zika, J.M., Heiple, K., Klein, L., 1975. Contribution of collagen and mineral to the elastic–plastic properties of bone. Journal of Bone and Joint Surgery 57, 956–961.

Carter, D.R., Hayes, W.C., 1977. The compressive behaviour of bone as a two-phase porous structure. Journal of Bone and Joint Surgery 59A, 954–962.

Choi, K., Kuhn, J., Ciarelli, M., Goldstein, S., 1990. The elastic moduli of human subchondral, trabecular, and cortical bone tissue and the size-dependency of cortical bone modulus. Journal of Biomechanics 23, 1103–1113.

Currey, J.D., 1984. Effects of differences in mineralization on the mechanical properties of bone. Philosophical Transactions of the Royal Society (London) B304, 509–518.

Currey, J.D., 1988. Strain rate and mineral content in fracture models of bone. Journal of Orthopaedic Research 6, 32–38.

Hengsberger, S., Kulik, A., Zysset, P.H., 2002. Nanoindentation discriminates the elastic properties of individual human bone lamellae under dry and physiological conditions. Bone 30, 178–184.

Hobatho, M.C., Rho, J.Y., Ashman, R.B., 1997. Anatomical variation of human cancellous bone mechanical properties in vitro. Studies in Health Technology and Information 40, 157–173.

Hoffler, C.E., Moore, K.E., Kozloff, K., Zysset, P.K., Brown, M.B., Goldstein, S.A., 2000. Heterogeneity of bone lamellar-level elastic moduli. Bone 26, 603–609.

Homminga, J., Huiskes, R., Van Rietbergen, B., Rüegsegger, P., Weinans, H., 2001. Introduction and evaluation of a gray-value voxel conversion technique. Journal of Biomechanics 34, 513–517.

Jaasma, M.J., Bayraktar, H.H., Niebur, G.L., Keaveny, T.M., 2002. Biomechanical effects of intraspecimen variations in tissue modulus for trabecular bone. Journal of Biomechanics 35, 237–246.

Jain, A., 1989. Fundamentals of Digital Image Processing. Prentice-Hall, Englewood Cliffs, NJ, p. 382.

Kabel, J., van Rietbergen, B., Dalstra, M., Odgaard, A., Huiskes, R., 1999. The role of an effective isotropic tissue modulus in the elastic properties of cancellous bone. Journal of Biomechanics 32, 673–680.

Keaveny, T.M., Guo, X.E., Wachtel, E.F., McMahon, T.A., Hayes, W.C., 1994. Trabecular bone exhibits fully linear elastic behavior and yields at low strains. Journal of Biomechanics 27, 1127–1136.

Kuhn, J.L., Goldstein, S.A., Choi, K., London, M., Feldkamp, L.A., Matthews, L.S., 1989. Comparison of the trabecular and cortical tissue moduli from human iliac crests. Journal of Orthopaedic Research 7, 876–884.

Ladd, A.J., Kinney, J.H., Haupt, D.L., Goldstein, S.A., 1998. Finite-element modeling of trabecular bone: comparison with mechanical testing and determination of tissue modulus. Journal of Orthopaedic Research 16, 622–628.

Morgan, T.G., van der Meulen, M.C., Bourne, B.C., 2002. Density versus depth from trabecular surface measured by quantitative microCT. Transactions of the Orthopaedic Research Society 27, 110.

Paschalis, E.P., Betts, F., DiCarlo, E., Mendelsohn, R., Boskey, A.L., 1997. FTIR microspectroscopic analysis of normal human cortical and trabecular bone. Calcified Tissue International 61, 480–486.

Rho, J.Y., Ashman, R.B., Turner, C.H., 1993. Young's modulus of trabecular and cortical bone material: ultrasonic and microtensile measurements. Journal of Biomechanics 26, 111–119.

Rho, J.Y., Tsui, T.Y., Pharr, G.M., 1997. Elastic properties of human cortical and trabecular lamellar bone measured by nanoindentation. Biomaterials 18, 1325–1330.

Rho, J.Y., Roy 2nd, M.E., Tsui, T.Y., Pharr, G.M., 1999. Elastic properties of microstructural components of human bone tissue as measured by nanoindentation. Journal of Biomedical Materials Research 45, 48–54.

Turner, C.H., Rho, J., Takano, Y., Tsui, T.Y., Pharr, G.M., 1999. The elastic properties of trabecular and cortical bone tissues are similar: results from two microscopic measurement techniques. Journal of Biomechanics 32, 437–441.

Ulrich, D., Hildebrand, T., Van Rietbergen, B., Müller, R., Rüegsegger, P., 1997. The quality of trabecular bone evaluated with micro-computed tomography, FEA and mechanical testing. Studies in Health Technology and Information 40, 97–112.

van der Linden, J.C., Birkenhager-Frenkel, D.H., Verhaar, J.A.N., Weinans, H., 2001. Trabecular bone's mechanical properties are affected by its non-uniform mineral distribution. Journal of Biomechanics 34, 1573–1580.

van Lenthe, G.H., van den Bergh, J.P., Hermus, A.R., Huiskes, R., 2001. The prospects of estimating trabecular bone tissue properties from the combination of ultrasound, dual-energy X-ray absorptiometry, microcomputed tomography, and microfinite element analysis. Journal of Bone and Mineral Research 16, 550–555.

van Rietbergen, B., Weinans, H., Huiskes, R., Odgaard, A., 1995. A new method to determine trabecular bone elastic properties and loading using micromechanical finite-element models. Journal of Biomechanics 28, 69–81.

van Rietbergen, B., Odgaard, A., Kabel, J., Huiskes, R., 1996. Direct mechanics assessment of elastic symmetries and properties of trabecular bone architecture. Journal of Biomechanics 29, 1653–1657.

van Rietbergen, B., Majumdar, S., Newitt, D., MacDonald, B., 2002. High-resolution MRI and micro-FE for the evaluation of changes in bone mechanical properties during longitudinal clinical trials: application to calcaneal bone in postmenopausal women after one year of idoxifene treatment. Clinical Biomechanics 17, 81–88.

Weiner, S., Arad, T., Sabanay, I., Traub, W., 1997. Rotated plywood structure of primary lamellar bone in the rat: orientations of the collagen fibril arrays. Bone 20, 509–514.

Ziv, V., Wagner, H.D., Weiner, S., 1996. Microstructure-microhardness relations in parallel-fibered and lamellar bone. Bone 18, 417–428.

Zysset, P.K., Guo, X.E., Hoffler, C.E., Moore, K.E., Goldstein, S.A., 1999. Elastic modulus and hardness of cortical and trabecular bone lamellae measured by nanoindentation in the human femur. Journal of Biomechanics 32, 1005–1012.